J. Plasma Phys. (2018), *vol.* 84, 905840112 © Cambridge University Press 2018
doi:10.1017/S0022377818000144

Electromagnetic responses of relativistic electrons

C. A. A. de Carvalho[1,2,†] **and D. M. Reis**[3]

[1]Diretoria-Geral de Desenvolvimento Nuclear e Tecnológico da Marinha – DGDNTM, Rua da Ponte, Ed. 23 do AMRJ, Rio de Janeiro – RJ, 20091-000, Brazil

[2]Instituto de Física, Universidade Federal do Rio de Janeiro – UFRJ, Caixa Postal 68528, Rio de Janeiro – RJ, 21945-972, Brazil

[3]Centro Brasileiro de Pesquisas Físicas – CBPF, Rua Dr. Xavier Sigaud 150, Rio de Janeiro – RJ, 22290-180, Brazil

(Received 1 September 2017; revised 16 January 2018; accepted 16 January 2018)

We compute the real and imaginary parts of the electric permittivities and magnetic permeabilities of relativistic electrons from quantum electrodynamics at finite temperatures and densities, for weak fields, neglecting electron–electron interactions. For non-zero temperatures, electromagnetic responses are reduced to one-dimensional integrals computed numerically. For zero temperature, we find analytic expressions for both their real/dispersive and imaginary/absorptive parts. As an application of our results, we obtain the dispersion relation for longitudinal electric plasmons. Present calculations support our recent claim that, at low frequencies and long wavelengths, the system will exhibit simultaneously negative electric and magnetic responses.

Key words: astrophysical plasmas, plasma properties, quantum plasma

1. Introduction

We have recently proposed (de Carvalho 2016) that a gas of relativistic electrons, in the long wavelength limit, for weak external fields and neglecting electron–electron (e–e) interactions, exhibits Drude-like expressions for both electric and magnetic responses. We then argued that the relativistic electron gas represents a natural realization of a material with simultaneously negative electric permittivity ϵ and magnetic permeability μ (Veselago 1968), (Pendry 2003).

As a test on the accuracy of our approximations (long wavelength, weak external fields, no e–e interactions), we have compared our predictions with non-relativistic data from metallic systems (Reyes-Gómez & de Carvalho 2016) and found that their quasi-free electrons exhibited responses that agreed well with the theoretical calculations at finite temperature, giving good estimates for physical quantities such as plasma frequencies. Clearly, the relativistic electron gases found in synchrotron beams or in astrophysical scenarios are examples of physical systems required to complete the verification of our theoretical predictions.

Quantum electrodynamics (QED) at finite temperatures and finite particle densities provides a unified treatment that relates electromagnetic responses to the well-known

† Email address for correspondence: carlos.aragao51@gmail.com

https://doi.org/10.1017/S0022377818000144 Published online by Cambridge University Press

polarization tensor (Akhiezer & Peletminskii 1960) with both vacuum and medium contributions. Thanks to that treatment, it has been established (de Carvalho 2016) that (i) all responses depend on three scalar functions (one for the vacuum; two for the medium), (ii) polarizations depend on both the electric and magnetic fields, just as magnetizations depend on both magnetic and electric fields and (iii) many aspects of the analysis of electric responses will carry over to the magnetic ones, due to the analogy between permittivities ϵ and inverse permeabilities $\nu \equiv \mu^{-1}$, among them the fact that both ϵ and ν exhibit Drude-like responses at low frequencies in the long wavelength limit.

The present article calculates the real and imaginary parts of the electromagnetic responses of relativistic electrons. At temperatures $T \neq 0$, the problem is reduced to one-dimensional (1-D) integrals which involve the Fermi–Dirac occupation numbers for electrons and positrons. At $T = 0$, however, as the occupation numbers become step functions, we obtain analytic expressions for the medium contributions.

Analytic results for the response functions of the relativistic electron gas at $T = 0$ have already appeared in the literature in the context of plasma physics (Jancovici 1962; Melrose & Hayes 1984; Barton 1990; Pulsifer & Kalman 1992; Barbaro & Quaglia 2005; McOrist & Weise 2007; Eliasson & Shukla 2011). Only expressions for the longitudinal and transverse parts of the electric permittivity, ϵ_L and ϵ_T, were derived.

It is worth noting that, in the non-relativistic case, electromagnetic responses depend on two independent functions, so that magnetic responses may be obtained from ϵ_L and ϵ_T. In the relativistic case, however, responses depend on three independent functions, one of which accounts for the vacuum contribution. It turns out that the vacuum contribution is negligible at low frequencies for typical electron densities, so one can obtain magnetic responses from electric ones.

Nonetheless, one might envisage situations of extremely low densities where the vacuum contributes at low frequencies. Also, at high frequencies, it does play a role. Thus, we present analytic results at $T = 0$ and numerical ones at $T \neq 0$ for electric permittivities and for magnetic permeabilities.

It should also be noted that finite temperature and density QED has been used by several authors to compute electromagnetic responses (Tsai & Erber 1974; Pérez Rojas & Shabad 1982; Weldon 1982; Donoghue & Robinett 1985; Ahmed & Masood 1991; Masood & Saleem 2016). Nevertheless, those articles do not obtain analytic expressions at $T = 0$ and concentrate on some limiting cases for $T \neq 0$.

Electromagnetic responses may be used to obtain the dispersion relation for plasmon modes that propagate when external electromagnetic fields induce resonant charge density collective oscillations in the electron gas. Such modes are present even when we neglect electron–electron interactions, as is well established in the condensed matter (Abrikosov & Dzyaloshinski 1975; Ashcroft & Mermin 2005; Fetter & Walecka 2012) and finite temperature field theory (Le Bellac 2000; Kapusta & Gale 2006) literatures.

In the particular case of longitudinal electric plasmon modes, used here as an example, the condition $\epsilon_L = 0$ leads to the desired dispersion relation, so we obtain the corresponding curve in the frequency–wavenumber plane. Furthermore, when the plasmon dispersion curve reaches the region where ϵ_L acquires an imaginary part, the plasmon decays into an electron–hole pair, with the hole corresponding to the absence of an electron in the Fermi sea (the region between mc^2 and the Fermi energy ε_F) (Sturm & Oliveira 1980, 1981; Sturm 1982). The imaginary part of ϵ_L allows for the calculation of decay times.

https://doi.org/10.1017/S0022377818000144 Published online by Cambridge University Press

The article is organized as follows: Section 2 derives electromagnetic responses from the polarization tensor of QED and expresses them in terms of three scalar functions. Section 3 derives the imaginary and real parts of the response functions for $T \neq 0$ in terms of 1-D integrals and in terms of analytic expressions for $T = 0$. Section 4 connects electromagnetic responses to collective plasmon excitations to obtain their dispersion relations. Finally, Section 5 presents our conclusions. Appendices A–D give details of the calculations in Section 3.

2. Electromagnetic responses from QED

A semiclassical expansion for the partition function Z of QED at finite temperature T with electron chemical potential ξ was derived in de Carvalho (2016). Its starting point was the expression for Z in terms of a path integral over the electromagnetic gauge fields and the electron fermionic fields, minimally coupled. The imaginary time formalism was used to implement the finite temperature condition. Throughout the derivation, natural units $\hbar = 1$, $c = 1$ and $k_B = 1$ were used.

The gauge field was then written as the sum of a classical field and a fluctuating quantum field. The quadratic integral over the quantum gauge field was performed giving rise to an effective Lagrangian with an electron–electron interaction term mediated by photons (the Coulomb interaction) and a lowest-order (in the quantum gauge field) term describing the electrons in interaction with the classical field. Integrating over the electron field yielded a fermionic determinant which was expanded in the classical gauge field, assumed to be weak. Only the lowest-order term in the expansion was kept, which is equivalent to the linear response approximation, and the electron–electron interaction was neglected, as it gave rise to higher-order terms in $\alpha \equiv \mathrm{e}^2/(4\pi) = 1/137$.

We were thus able to write an effective action for the classical gauge field. We extremized it to obtain equations of motion that took into account the presence of the medium. The overall effect was to add an induced current as a source for Maxwell's equations, which in turn led to the polarization and magnetization of the electron gas through the momentum-space equation

$$\mathrm{i}q_\mu \tilde{P}_{\mu\nu}(q) = \tilde{\Pi}_{\nu\sigma}(q)\tilde{A}_\sigma(q). \tag{2.1}$$

The Euclidean space $P_{\mu\nu}$ encodes the polarization $\boldsymbol{P}$ ($P_{4j} = \mathrm{i}P_j$) and magnetization $\boldsymbol{M}$ ($P_{ij} = -\epsilon_{ijk}M_k$) vectors. $\tilde{\Pi}_{\nu\sigma}(q)$ is the one-loop polarization tensor of QED (Akhiezer & Peletminskii 1960)

$$\tilde{\Pi}_{\mu\nu} = -\frac{\mathrm{e}^2}{\beta}\sum_{n=-\infty}^{+\infty}\int\frac{\mathrm{d}^3p}{(2\pi)^3}\mathrm{Sp}[\gamma_\mu G_0(p)\gamma_\nu G_0(p-q)], \tag{2.2}$$

where $\beta = T^{-1}$, the sum is over Matsubara frequencies $p_4 = (2n+1)\pi T$, G_0 is the free electron propagator and Sp denotes trace over Dirac matrices. Equation (2.1) implies

$$\tilde{P}_{\mu\nu} = \frac{\tilde{\Pi}_{\mu\sigma}}{q^2}\tilde{F}_{\nu\sigma} - \frac{\tilde{\Pi}_{\nu\sigma}}{q^2}\tilde{F}_{\mu\sigma}, \tag{2.3}$$

so that polarization and magnetization are related to the fields $\boldsymbol{E}$ ($\tilde{F}_{4j} = \mathrm{i}\tilde{E}^j$) and $\boldsymbol{B}$ ($\tilde{F}_{ij} = \epsilon_{ijk}\tilde{B}^k$), thus yielding electric and magnetic susceptibilities and, ultimately, electric permittivities and magnetic permeabilities.

https://doi.org/10.1017/S0022377818000144 Published online by Cambridge University Press

One may write $\tilde{\Pi}_{\nu\sigma} = \tilde{\Pi}^{(v)}_{\nu\sigma} + \tilde{\Pi}^{(m)}_{\nu\sigma}$ to separate vacuum ($T = \xi = 0$) and medium contributions. The vacuum contribution has the structure

$$-\frac{\tilde{\Pi}^{(v)}_{\nu\sigma}}{q^2} = \left(\delta_{\nu\sigma} - \frac{q_\nu q_\sigma}{q^2}\right) \mathcal{C}(q^2). \tag{2.4}$$

The medium, however, introduces a preferred reference frame (that of its centre of mass). The symmetry of the problem is then reduced to three-dimensional rotation and gauge invariance, leading to

$$-\frac{\tilde{\Pi}^{(m)}_{ij}}{q^2} = \left(\delta_{ij} - \frac{q_i q_j}{|\boldsymbol{q}|^2}\right) \mathcal{A} + \delta_{ij} \frac{q_4^2}{|\boldsymbol{q}|^2} \mathcal{B}, \tag{2.5}$$

$$-\frac{\tilde{\Pi}^{(m)}_{44}}{q^2} = \mathcal{B}, \quad -\frac{\tilde{\Pi}^{(m)}_{4i}}{q^2} = -\frac{q_4 q_i}{|\boldsymbol{q}|^2} \mathcal{B}, \tag{2.6a,b}$$

where the three scalar functions $\mathcal{A}(q_4, |\boldsymbol{q}|)$, $\mathcal{B}(q_4, |\boldsymbol{q}|)$ and $\mathcal{C}(q^2)$ are determined from the Feynman graph in (2.2), the QED polarization tensor at finite temperature and density computed long ago (Akhiezer & Peletminskii 1960).

$\mathcal{A}$ and $\mathcal{B}$ are calculated from the trace, $\tilde{\Pi}_{\mu\mu}$, and from $\tilde{\Pi}_{44}$, once we subtract the vacuum part, i.e.

$$\mathcal{A} = \frac{-\mathrm{e}^2}{2\pi^3 q^2} \mathrm{Re} \int \frac{\mathrm{d}^3 p}{\varepsilon_p} n_F(p) \frac{p \cdot (p+q)}{q^2 - 2p \cdot q} + \left(1 - \frac{3q^2}{2|\boldsymbol{q}|^2}\right) \mathcal{B}, \tag{2.7}$$

$$\mathcal{B} = \frac{-\mathrm{e}^2}{2\pi^3 q^2} \mathrm{Re} \int \frac{\mathrm{d}^3 p}{\varepsilon_p} n_F(p) \frac{p \cdot q - 2p_4(q_4 - p_4)}{q^2 - 2p \cdot q}, \tag{2.8}$$

where $p_4 = \mathrm{i}\varepsilon_p = \mathrm{i}\sqrt{|\boldsymbol{p}|^2 + m^2}$, while $n_F(p)$ is the Fermi–Dirac occupation number for particles and antiparticles,

$$n_F(p) = \frac{1}{\mathrm{e}^{\beta(\varepsilon_p - \xi)} + 1} + \frac{1}{\mathrm{e}^{\beta(\varepsilon_p + \xi)} + 1}. \tag{2.9}$$

We now introduce $H_{\mu\nu} \equiv F_{\mu\nu} + P_{\mu\nu}$, which defines $H_{4j} = \mathrm{i}D_j$ and $H_{ij} = \epsilon_{ijk} H_k$, with $\boldsymbol{D} = \boldsymbol{E} + \boldsymbol{P}$ and $\boldsymbol{H} = \boldsymbol{B} - \boldsymbol{M}$. The constitutive equations are derived from (2.4), (2.5) and (2.6), i.e.

$$\tilde{D}_j = \epsilon_{jk} \tilde{E}_k + \tau_{jk} \tilde{B}_k, \tag{2.10}$$

$$\tilde{H}_j = \nu_{jk} \tilde{B}^k + \tau_{jk} \tilde{E}_k, \tag{2.11}$$

where we have defined $\nu_{jk} \equiv (\mu^{-1})_{jk}$ as the inverse of the magnetic permeability tensor. Using $\hat{q}^i \equiv q^i / |\boldsymbol{q}|$, we obtain

$$\epsilon_{jk} = \epsilon \delta_{jk} + \epsilon' \hat{q}_j \hat{q}_k, \tag{2.12}$$

$$\nu_{jk} = \nu \delta_{jk} + \nu' \hat{q}_j \hat{q}_k, \tag{2.13}$$

$$\tau_{jk} = \tau \epsilon_{jkl} \hat{q}_l. \tag{2.14}$$

Again, $\nu \equiv \mu^{-1}$, $\nu' \equiv \mu'^{-1}$. One should stress that there are contributions to $(\boldsymbol{D}, \boldsymbol{H})$ along the directions of the fields $(\boldsymbol{E}, \boldsymbol{B})$, of the wave vector $\boldsymbol{q}$, and of $(\boldsymbol{q} \wedge \boldsymbol{B}, \boldsymbol{q} \wedge \boldsymbol{E})$;

https://doi.org/10.1017/S0022377818000144 Published online by Cambridge University Press

also note that bianisotropic crystals satisfy similar relations (Berry 2005; Gu & Yin 2014).

The permittivities and inverse permeabilities

$$\epsilon = 1 + \left(2 - \frac{\omega^2}{q^2}\right)\mathcal{C}^* + \mathcal{A}^* + \left(1 - \frac{\omega^2}{|\boldsymbol{q}|^2}\right)\mathcal{B}^*, \tag{2.15}$$

$$\nu = 1 + \left(2 + \frac{|\boldsymbol{q}|^2}{q^2}\right)\mathcal{C}^* + \mathcal{A}^* - 2\frac{\omega^2}{|\boldsymbol{q}|^2}\mathcal{B}^*, \tag{2.16}$$

$$\epsilon' = -\nu' = \frac{|\boldsymbol{q}|^2}{q^2}\mathcal{C}^* - \mathcal{A}^*; \quad \tau = \frac{\omega}{|\boldsymbol{q}|}\left(\frac{|\boldsymbol{q}|^2}{q^2}\mathcal{C}^* - \mathcal{B}^*\right), \tag{2.17a,b}$$

are determined by the three scalar functions $\mathcal{A}^*$, $\mathcal{B}^*$ and $\mathcal{C}^*$. The asterisk indicates that we have continued from Euclidean to Minkowski space by letting $q_4 \to \mathrm{i}\omega - 0^+$ in $\mathcal{A}$, $\mathcal{B}$, and $\mathcal{C}$. Likewise, the Euclidean $q^2 \equiv q_4^2 + |\boldsymbol{q}|^2$ goes to $-q^2 \equiv -\omega^2 + |\boldsymbol{q}|^2$, since we use the Minkowski metric $(-, +, +, +)$.

$\mathcal{C}^*$ may be obtained from the standard calculation at $T = \xi = 0$ (Itzykson & Zuber 2006).

$$\mathcal{C}^* = \frac{-\mathrm{e}^2}{12\pi^2}\left\{\frac{1}{3} + 2\left(1 + \frac{2m^2}{q^2}\right)\left[\sqrt{(4m^2/q^2) - 1}\,\mathrm{arccot}\left(\sqrt{(4m^2/q^2) - 1}\right) - 1\right]\right\}. \tag{2.18}$$

The renormalization condition is $\mathrm{e}^2/(4\pi) = 1/137$, with $\mathrm{e}^2 = \mathrm{e}^2(\omega = 0, \boldsymbol{q} = \boldsymbol{0})$. The vacuum contributions to permittivities and inverse permeabilities are obtained by setting $\mathcal{A}^* = \mathcal{B}^* = 0$.

For further discussions, it is important to diagonalize the tensors appearing in (2.12), (2.13). For ϵ_{jk}, the eigenvalues λ satisfy $\det(\epsilon_{jk} - \lambda\delta_{jk}) = 0$, leading to $(\epsilon - \lambda)^2(\epsilon + \epsilon' - \lambda) = 0$. The eigenvector associated with $\epsilon + \epsilon'$ is $\hat{q}_k$, so that it is longitudinal, whereas the two eigenvalues ϵ are transverse to $\hat{q}_k$. The same occurs for ν_{jk}. Therefore, from (2.15), (2.16)

$$\epsilon_L = \epsilon + \epsilon' = 1 + \mathcal{C}^* + \left(1 - \frac{\omega^2}{|\boldsymbol{q}|^2}\right)\mathcal{B}^*, \tag{2.19}$$

$$\nu_L = \nu + \nu' = 1 + 2\left(\mathcal{C}^* + \mathcal{A}^* - \frac{\omega^2}{|\boldsymbol{q}|^2}\mathcal{B}^*\right). \tag{2.20}$$

Whenever $\mathcal{C}^*$ is negligible with respect to $\mathcal{A}^*$ and $\mathcal{B}^*$, the longitudinal ϵ_L and transverse ϵ_T electric permittivities may be used to compute $\mathcal{A}^*$ and $\mathcal{B}^*$. Indeed, $\mathcal{A}^* = \epsilon_T - \epsilon_L$ and $\mathcal{B}^* = (|\boldsymbol{q}|^2/q^2)(1 - \epsilon_L)$. In this case, we will have $\nu_L = \nu_L(\epsilon_L, \epsilon_T)$ and $\nu_T = \nu_T(\epsilon_L, \epsilon_T)$, as in non-relativistic systems. Figure 1 exhibits situations where the vacuum makes a relevant contribution to the longitudinal permittivity ϵ_L.

3. Real and imaginary parts of the responses

We will now explicitly compute the real and imaginary parts of the expressions for longitudinal responses both at $T \neq 0$ and at $T = 0$. For that purpose, it is convenient to define the integral in (2.7), continued to Minkowski space, as a new quantity $\mathcal{D}^*$

$$\mathcal{D}^* = \mathcal{A}^* - \left[1 + \frac{3q^2}{2|\boldsymbol{q}|^2}\right]\mathcal{B}^*. \tag{3.1}$$

https://doi.org/10.1017/S0022377818000144 Published online by Cambridge University Press

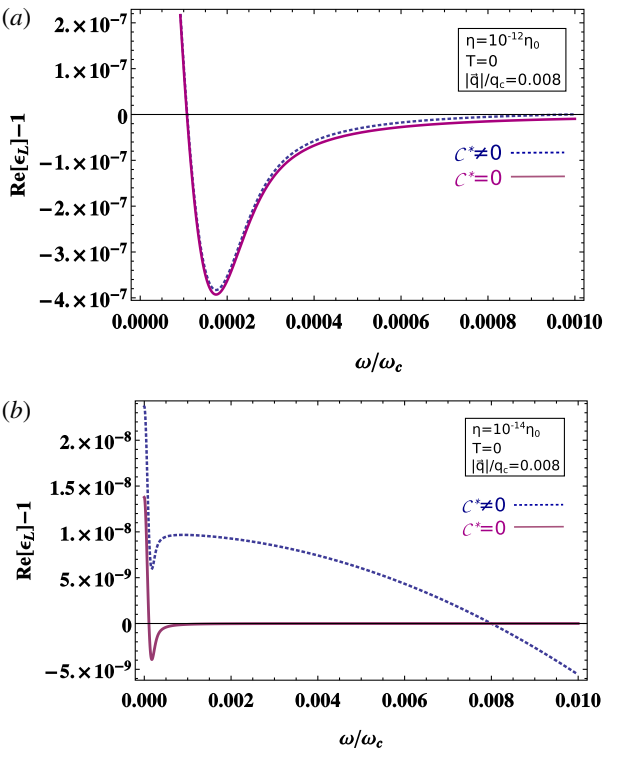


FIGURE 1. Plot of $(\mathrm{Re}[\epsilon_L]-1)$ for low densities of the electron gas at $T=0$. The dashed line has the vacuum contribution ($\mathcal{C}^* \neq 0$), whereas the full line only has the medium contribution ($\mathcal{C}^*=0$). (*a*) Electron density $\eta = 10^{-12}\eta_0$ and (*b*) $\eta = 10^{-14}\eta_0$, where $\eta_0 \approx 1.76 \times 10^{30}$ cm^{-3}. Both the frequency and wave vector are given in units of $\omega_c = mc^2/\hbar$, the Compton frequency, and $q_c = mc/\hbar$, the Compton wave vector.

Integration over angles and continuation to Minkowski space ($q_4 \to \mathrm{i}\omega - 0^+$) lead to

$$\mathcal{B}^* = \frac{-\mathrm{e}^2}{\pi^2 q^2}\int_0^\infty \frac{\mathrm{d}p p^2 n_F}{\varepsilon_p}\left[1+\frac{4\varepsilon_p^2+q^2}{8p|\boldsymbol{q}|}L_1+\frac{\varepsilon_p\omega}{p|\boldsymbol{q}|}L_2\right], \tag{3.2}$$

$$\mathcal{D}^* = \frac{-\mathrm{e}^2}{\pi^2 q^2}\int_0^\infty \frac{\mathrm{d}p\, p^2 n_F}{\varepsilon_p}\left[1+\frac{2m^2+q^2}{8p|\boldsymbol{q}|}L_1\right]. \tag{3.3}$$

The functions L_1 and L_2 are given by

$$L_1 = \ln\left\{\frac{(\chi^2-by)^2-a^2x^2}{(\chi^2+by)^2-a^2x^2}\right\}; \tag{3.4}$$

$$L_2 = \ln\left\{\left|\frac{\chi^2-by+ax}{\chi^2+by+ax}\right|\right\} - \frac{L_1}{2}, \tag{3.5}$$

where we have used dimensionless variables $x \equiv \varepsilon_p/m$, $y \equiv p/m = \sqrt{x^2-1}$, $a \equiv \omega/2m$, $b \equiv |\boldsymbol{q}|/2m$, and $\chi^2 \equiv a^2 - b^2 = q^2/4m^2$.

https://doi.org/10.1017/S0022377818000144 Published online by Cambridge University Press

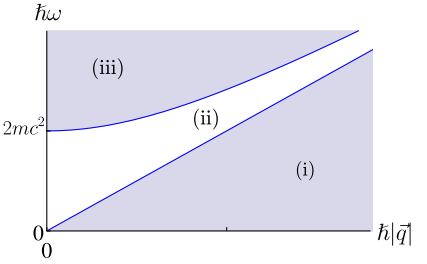


FIGURE 2. Regions of the $(a, b) \sim (\hbar\omega, \hbar|\boldsymbol{q}|)$ plane where the imaginary parts of the responses are given by different expressions. In region (ii), they always vanish, whereas in regions (i) and (iii) they are given by (3.10) and (3.11).

3.1. *Real parts at* $T \neq 0$

The real parts of $\mathcal{B}^*$ and $\mathcal{D}^*$ reduce to 1-D integrals. We write them as

$$\mathrm{Re}\,\mathcal{B}^* = \frac{-\mathrm{e}^2}{4\pi^2\chi^2}\left(\int_1^\infty \mathrm{d}x n_F\sqrt{x^2-1} + \frac{1}{4b}\int_1^\infty \mathrm{d}x n_F[(x^2+\chi^2)R_1 + 4axR_2]\right), \quad (3.6)$$

$$\mathrm{Re}\,\mathcal{D}^* = \frac{-\mathrm{e}^2}{4\pi^2\chi^2}\left(\int_1^\infty \mathrm{d}x n_F\sqrt{x^2-1} + \frac{1}{8b}\int_1^\infty \mathrm{d}x n_F(1+2\chi^2)R_1\right), \quad (3.7)$$

with $R_1 \equiv \mathrm{Re}\,L_1$ and $R_2 \equiv \mathrm{Re}\,L_2$. Since $\mathcal{C}^*$ is real, we obtain

$$\mathrm{Re}\,\epsilon_L = 1 + \mathcal{C}^* - \frac{\chi^2}{b^2}\mathrm{Re}\,\mathcal{B}^*, \quad (3.8)$$

$$\mathrm{Re}\,\nu_L = 1 + 2\mathcal{C}^* + 2\mathrm{Re}\,\mathcal{D}^* + \frac{\chi^2}{b^2}\mathrm{Re}\,\mathcal{B}^*. \quad (3.9)$$

The results above allow for the calculation of plasmon dispersion relations, as we will show later on.

3.2. *Imaginary parts at* $T \neq 0$

From the calculations in appendix A, defining $\eta^2 \equiv 1 - (1/\chi^2)$, we identify three regions in the (a, b) plane

(i) $\chi^2 < 0$ $(\eta > 1;\ a < b < b\eta)$: $-a + b\eta < x < a + b\eta$;
(ii) $0 < \chi^2 < 1$ (η pure imaginary): the condition is never satisfied and $\mathrm{Im}\,L_1 = 0$;
(iii) $\chi^2 > 1$ $(\eta < 1;\ a > b > b\eta)$: $a - b\eta < x < a + b\eta$.

They are shown in figure 2. For the longitudinal responses, we have

$$\mathrm{Im}\,\epsilon_L = -\frac{\mathrm{sign}(\chi^2)\mathrm{e}^2}{16\pi b^3}\int_{x_l}^{a+b\eta} \mathrm{d}x n_F[(x-a)^2 - b^2] \quad (3.10)$$

$$\mathrm{Im}\,\nu_L = \frac{\mathrm{sign}(\chi^2)\mathrm{e}^2}{16\pi b\chi^2}\int_{x_l}^{a+b\eta} \mathrm{d}x n_F(1+2\chi^2) - \mathrm{Im}\,\epsilon_L. \quad (3.11)$$

$\mathrm{Im}\,\nu_L$ and $\mathrm{Im}\,\epsilon_L$ vanish in region (ii) of the (a, b) plane. In region (i) $x_l = -a + b\eta$ and in region (iii) $x_l = a - b\eta$. Using the expressions for the imaginary parts in

https://doi.org/10.1017/S0022377818000144 Published online by Cambridge University Press

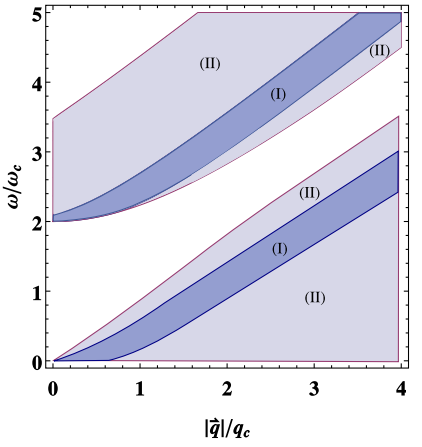


FIGURE 3. Evolution with temperature of the regions of the $(a, b) \sim (\hbar\omega, \hbar|\boldsymbol{q}|)$ plane with non-vanishing imaginary parts. As $\tilde{\beta}$ decreases, the two $T = 0$ regions (labelled I) expand. For a value of $\tilde{\beta} = 10^3$, imaginary parts appear in all regions labelled I and II. Eventually, as $T \to \infty$, only the unshaded region of figure 2 will have vanishing imaginary parts.

regions (i) and (iii), we may see how their values evolve from $T = 0$ to non-zero temperatures. This is shown in figure 3. One should note that the appearance of non-zero imaginary parts is associated with the creation of electron–hole (lower energies) or electron–positron (higher energies) pairs.

We have thus derived electromagnetic responses as functions of a, b, T/m and ξ/m, the two latter dependences from coming from the Fermi–Dirac distribution function.

3.3. *Imaginary parts at* $T = 0$

At $T = 0$, $n_F(x) \to \Theta(x_F - x)$, with $x_F \equiv \varepsilon_F/m = \xi/m$ and $y_F = (1/m)\sqrt{\varepsilon_F^2 - m^2} = p_F/m$. We may then analytically perform the integrals for both the imaginary and real parts of the response functions. Additional restrictions come into play because of the integration limit x_F imposed by the function $\Theta(x_F - x)$.

From the calculations in appendix A, we identify four regions in the (a, b) plane where the longitudinal responses will have different values. We use $[f(x)]_{x_l}^{x_u} \equiv f(x_u) - f(x_l)$ and refer the reader to the appendix B for the calculation of $b_\pm$, $\bar{b}_\pm$, $b'_\pm$ and $\bar{b}'_\pm$. The regions are

(A) for $0 < a < (x_F - 1)/2$ and $(x_F + 1)/2 < a < x_F$, $\bar{b}_- < b < \bar{b}_+$, $x_l = -a + b\eta$, $x_u = a + b\eta$,

$$\left.\begin{aligned} \mathrm{Im}\,\epsilon_L &= \frac{\mathrm{e}^2}{48\pi b^3}[(x-a)^3 - 3b^2x]_{-a+b\eta}^{a+b\eta}, \\ \mathrm{Im}\,\nu_L &= -\frac{\mathrm{e}^2}{16\pi b\chi^2}[2a(1+2\chi^2)] - \mathrm{Im}\,\epsilon_L; \end{aligned}\right\} \tag{3.12}$$

(B) for $(x_F - 1)/2 < a < (x_F + 1)/2$ and $a > x_F$, $b_- < b < b_+$, $x_l = -a + b\eta$, $x_u = x_F$,

$$\left.\begin{aligned} \mathrm{Im}\,\epsilon_L &= \frac{\mathrm{e}^2}{48\pi b^3}[(x-a)^3 - 3b^2x]_{-a+b\eta}^{x_F}, \\ \mathrm{Im}\,\nu_L &= -\frac{\mathrm{e}^2}{16\pi b\chi^2}[(x_F + a - b\eta)(1+2\chi^2)] - \mathrm{Im}\,\epsilon_L. \end{aligned}\right\} \tag{3.13}$$

https://doi.org/10.1017/S0022377818000144 Published online by Cambridge University Press

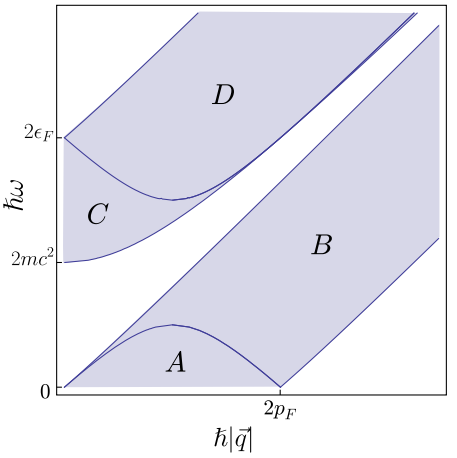


FIGURE 4. Regions in the $(a, b) \sim (\hbar\omega, \hbar|\boldsymbol{q}|)$ plane where the imaginary parts are non-vanishing for $T = 0$. The limits of regions A, B, C, D and the values of the longitudinal responses in each of them are shown in § 3.3.

Outside regions (A) and (B), for $\chi^2 < 0$ the imaginary parts of ϵ_L and ν_L vanish.

(C) for $0 < a < (x_F - 1)/2$ and $(x_F + 1)/2 < a < x_F$, $\bar{b}'_- < b < \bar{b}'_+$, $x_l = a - b\eta$, $x_u = a + b\eta$,

$$\left.\begin{aligned} \operatorname{Im}\epsilon_L &= -\frac{\mathrm{e}^2}{48\pi b^3}[(x-a)^3 - 3b^2 x]_{a-b\eta}^{a+b\eta}, \\ \operatorname{Im}\nu_L &= \frac{\mathrm{e}^2}{16\pi b\chi^2}[2b\eta(1+2\chi^2)] - \operatorname{Im}\epsilon_L; \end{aligned}\right\} \tag{3.14}$$

(D) for $(x_F - 1)/2 < a < (x_F + 1)/2$ and $a > x_F$, $b'_- < b < b'_+$, $x_l = a - b\eta$, $x_u = x_F$,

$$\left.\begin{aligned} \operatorname{Im}\epsilon_L &= -\frac{\mathrm{e}^2}{48\pi b^3}[(x-a)^3 - 3b^2 x]_{a-b\eta}^{x_F}, \\ \operatorname{Im}\nu_L &= \frac{\mathrm{e}^2}{16\pi b\chi^2}[(x_F - a + b\eta)(1+2\chi^2)] - \operatorname{Im}\epsilon_L. \end{aligned}\right\} \tag{3.15}$$

Outside regions (C) and (D), for $\chi^2 > 1$ the imaginary parts of ϵ_L and ν_L vanish.

Finally, in case (ii), $0 < \chi^2 < 1$, one has $\operatorname{Im}\epsilon_L = \operatorname{Im}\nu_L = 0$.

The various regions of the (a,b) plane that correspond to the different expressions discussed above are depicted in figure 4.

3.4. *Real parts at* $T = 0$

For the real parts at $T = 0$, we replace n_F with $\Theta(x_F - x)$ in (3.6) and (3.7). The calculations detailed in appendices C and D lead to

$$\operatorname{Re}\mathcal{B}^* = \frac{-\mathrm{e}^2}{4\pi^2\chi^2}[X_B + Y_B + Z_B], \tag{3.16}$$

$$\operatorname{Re}\mathcal{D}^* = \frac{-\mathrm{e}^2}{4\pi^2\chi^2}[X_D + Y_D + Z_D], \tag{3.17}$$

https://doi.org/10.1017/S0022377818000144 Published online by Cambridge University Press

where X_B, X_D, Y_B and Y_D are given by ($R_i = \mathrm{Re}\, L_i$; (3.4), (3.5))

$$X_B = \frac{x_F}{12b}[(x_F^2 + 3\chi^2)R_1(x_F) + 6ax_F R_2(x_F)], \tag{3.18}$$

$$X_D = \frac{x_F}{8b}(1 + 2\chi^2)R_1(x_F), \tag{3.19}$$

$$Y_B = \tfrac{2}{3}[x_F y_F - b^2 \ln(x_F + y_F)], \tag{3.20}$$

$$Y_D = \tfrac{1}{2}[x_F y_F + 2\chi^2 \ln(x_F + y_F)], \tag{3.21}$$

whereas Z_B and Z_D are given by

$$Z_{B,D} = C_{B,D}[(M_{B,D} + N_{B,D})\mathfrak{I}_0 - N_{B,D}\mathfrak{I}_2]. \tag{3.22}$$

$C_{B,D}(a, b)$, $M_{B,D}(a, b)$, $N_{B,D}(a, b)$ and the integrals $\mathfrak{I}_0(a, b, x_F)$ and $\mathfrak{I}_2(a, b, x_F)$ are defined and calculated in the appendix D.

The longitudinal responses (2.19) and (2.20) are given by

$$\mathrm{Re}\, \epsilon_L = 1 + \mathcal{C}^* + \frac{\mathrm{e}^2}{4\pi^2 b^2}[X_B + Y_B + Z_B], \tag{3.23}$$

$$\mathrm{Re}\, \nu_L = 1 + 2\mathcal{C}^* - \frac{\mathrm{e}^2}{2\pi^2\chi^2}[X_D + Y_D + Z_D] - \frac{\mathrm{e}^2}{4\pi^2 b^2}[X_B + Y_B + Z_B]. \tag{3.24}$$

4. Plasmon excitations

As mentioned in the introduction, electromagnetic responses may be used to obtain the dispersion relation for plasmon modes that propagate when external electromagnetic fields induce resonant charge density collective oscillations in the electron gas. The dispersion relation for longitudinal electric plasmons, for instance, is obtained from the well-known condition $\epsilon_L = 0$ (Abrikosov & Dzyaloshinski 1975; Sturm & Oliveira 1980, 1981; Sturm 1982; Fetter & Walecka 2012). As an application of our formulae, we will use our expressions for $\mathrm{Re}\, \epsilon_L$ and $\mathrm{Im}\, \epsilon_L$ to obtain it.

The solutions to $\mathrm{Re}\, \epsilon_L = 0$ are plotted in figure 5(*a*,*b*), for the case $T \neq 0$ and $T = 0$. Since we must have $\epsilon_L = 0$, the full curve in the figure is the physical one, because most of it lies in the unshaded region, where we also have $\mathrm{Im}\, \epsilon_L = 0$. The dashed curve lies completely in the region where there is an imaginary part, so that it never satisfies $\epsilon_L = 0$.

The shaded region in figure 5(*b*) is the same as the lower region of figure 4, where $\mathrm{Im}\, \epsilon_L \neq 0$. The dashed curve is fully within that region and thus a decaying mode, whereas the full curve lies mostly in the region where $\mathrm{Im}\, \epsilon_L = 0$. Thus, it describes a plasmon mode. As the curve enters the region where there is an imaginary part, the plasmon mode becomes unstable to the decay into electron–hole pairs, just as in the non-relativistic case.

Analytic results at $T = 0$ and numerical results at $T \neq 0$ may be used to compute decay constants and dispersion relations for both longitudinal and transverse plasmons. A complete discussion of the modes that propagate in the relativistic electron gas will appear elsewhere (Reis & de Carvalho 2017).

One may use our expressions to confirm that, for long wavelengths and below their plasmon frequencies, both ϵ_L and ν_L will be simultaneously negative, a behaviour previously thought to occur only in artificially nanoengineered materials. Our calculations show that this behaviour is natural in relativistic systems, where magnetic effects are not suppressed by v/c, unlike what happens in the non-relativistic limit, where $\nu_L \sim 1$.

https://doi.org/10.1017/S0022377818000144 Published online by Cambridge University Press

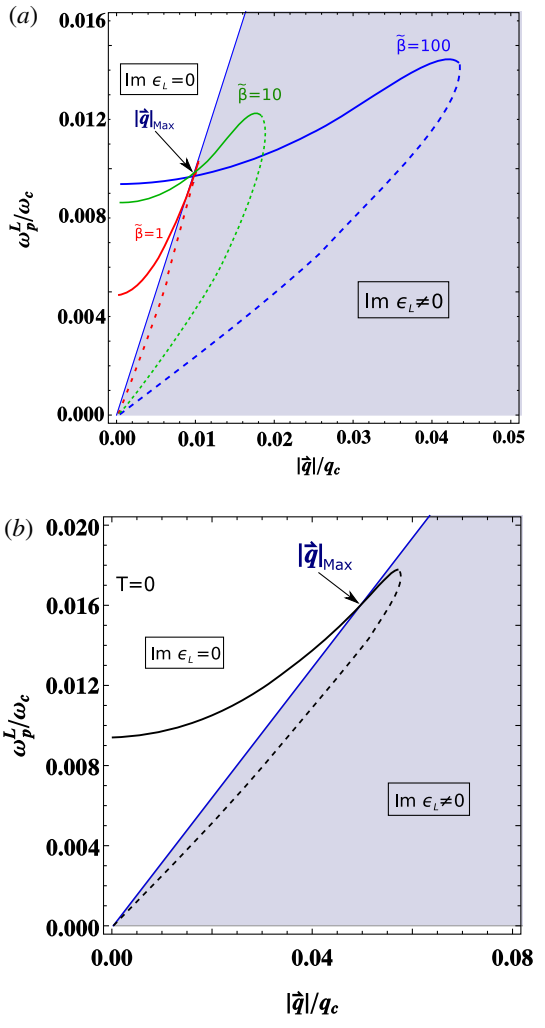


FIGURE 5. Upper (ω_p^L plasmon frequency) and lower frequency zeroes of ϵ_L (Solid and dashed lines, respectively) as functions of the $|\boldsymbol{q}|$ wave vector. Calculations were performed for (*a*) $\tilde{\beta} = 100$, $\tilde{\beta} = 10$, $\tilde{\beta} = 1$ and (*b*) $\tilde{\beta} \to \infty (T = 0)$ by taking the density electron gas $\eta = 10^{-2}\eta_0$, where $\eta_0 \approx 1.76 \times 10^{30}$ cm^{-3}. The shaded area corresponds to the region where electron–hole excitations occur. Note the maximum value of the wave vector ($|\boldsymbol{q}|_{max}$) beyond which the longitudinal plasmon decays into electron-hole pairs.

5. Conclusions

The unified treatment provided by QED at finite temperature and density allows one to relate the electromagnetic responses of the relativistic electron gas to the polarization tensor of QED which incorporates vacuum and medium effects. This is a first-principle calculation that opens up interesting possibilities, since the computation can be extended to other systems and to different dimensions.

We have thus used QED to compute the real and imaginary parts of both the electric and magnetic longitudinal responses of the relativistic electron gas. One may show that the non-relativistic limit of the present theoretical results for the dielectric

https://doi.org/10.1017/S0022377818000144 Published online by Cambridge University Press

response coincide with the celebrated Lindhard dielectric function (Lindhard 1954). For $T = 0$, we obtain analytic expressions that coincide with those existing in the literature if we neglect the vacuum contributions.

The appearance of non-zero imaginary parts indicates that the system is unstable to the decay into electron–hole (lower energies) or electron–positron (higher energies) pairs (Tsai & Erber 1974; Pulsifer & Kalman 1992). The former is well known to occur in the non-relativistic limit. Furthermore, the explicit expressions for longitudinal electric and magnetic responses allow for the calculation of dispersion relations for plasmons.

We hope that experimental data from synchrotron beams or observational data from astrophysical scenarios will allow us to test our predictions, just as we have done in Condensed Matter systems (Reyes-Gómez & de Carvalho 2016).

Acknowledgements

The authors wish to thank L. E. Oliveira for many fruitful discussions, for a critical reading of the manuscript, and for his warm hospitality at the Institute of Physics of the Universidade Estadual de Campinas, where part of this work was done. Thanks are also due to E. Reyes-Gómez for discussions and help with the figures, and to CAPES, CNPq and FAPESP for financial support.

Appendix A. Imaginary parts at $T \neq 0$

The vacuum contribution does not have an imaginary part. On the other hand, imaginary parts for $\mathcal{B}^*$ and $\mathcal{D}^*$ will appear whenever the argument in L_1 becomes negative (note that $\mathrm{Im}\, L_2 = -\mathrm{Im}\, L_1/2$). For that to occur, the product of the numerator $\mathfrak{N}$ times the denominator $\mathfrak{D}$ of the argument must satisfy,

$$\mathfrak{N}\mathfrak{D} = [(\chi^2 - by)^2 - a^2x^2][(\chi^2 + by)^2 - a^2x^2] < 0. \tag{A 1}$$

The roots of the related biquadratic equation in x ($\geqslant 0$) are $x_\pm = a \pm b\eta$, where $\eta^2 \equiv 1 - (1/\chi^2)$, leading to the condition $(a - b\eta)^2 < x^2 < (a + b\eta)^2$.

Three cases have to be considered:

(i) $\chi^2 < 0$ ($\eta > 1$; $a < b < b\eta$): $-a + b\eta < x < a + b\eta$;
(ii) $0 < \chi^2 < 1$ (η pure imaginary): the condition is never satisfied and $\mathrm{Im}\, L_1 = 0$;
(iii) $\chi^2 > 1$ ($\eta < 1$; $a > b > b\eta$): $a - b\eta < x < a + b\eta$.

The difference between numerator $\mathfrak{N}$ and denominator $\mathfrak{D}$ is given by $-\chi^2 by$. For case (i), this implies $\mathfrak{N} > 0$, $\mathfrak{D} < 0$ whereas for case (iii) $\mathfrak{N} < 0$, $\mathfrak{D} > 0$. For case (ii), $0 < \chi^2 < 1$, corresponding to the same sign for $\mathfrak{N}$ and $\mathfrak{D}$, $\mathrm{Im}\, \mathcal{B}^* = \mathrm{Im}\, \mathcal{D}^* = 0$.

For cases (i) and (iii), we take $\mathrm{Im}\, L_1 = \mathrm{sign}(\mathfrak{N})\pi$. The choice of sign corresponds to the continuation $q_4 \to \mathrm{i}\omega - 0^+$. Therefore

$$\mathrm{Im}\, \mathcal{B}^* = \frac{\mathrm{sign}(\chi^2)\mathrm{e}^2}{16\pi b\chi^2} \int_{x_l}^{a+b\eta} \mathrm{d}x n_F[(x-a)^2 - b^2] \tag{A 2}$$

$$\mathrm{Im}\, \mathcal{D}^* = \frac{\mathrm{sign}(\chi^2)\mathrm{e}^2}{32\pi b\chi^2} \int_{x_l}^{a+b\eta} \mathrm{d}x n_F(1 + 2\chi^2). \tag{A 3}$$

For case (i), $\chi^2 < 0$, $\mathfrak{N} > 0$, and $x_l = -a + b\eta$ whereas for case (iii), $\chi^2 > 1$, $\mathfrak{N} < 0$, and $x_l = a - b\eta$. It is easy to show that $-a + b\eta > 1$ in case (i) and $a - b\eta > 1$ in case (iii). Thus, imaginary parts may appear for both $\mathcal{B}^*$ and $\mathcal{D}^*$ in the regions $\chi^2 < 0$ and $\chi^2 > 1$ of the (a, b) plane, but they vanish for $0 < \chi^2 < 1$.

https://doi.org/10.1017/S0022377818000144 Published online by Cambridge University Press

Appendix B. Imaginary parts at $T = 0$

Again, the vacuum contribution does not have an imaginary part. We then refer to the three cases described in § 3.2, which correspond to different regions in the (a, b) plane.

In case (i), $\chi^2 < 0$, $\eta > 1$, $a < b < b\eta$, the lower integration limit of (A 2), (A 3) is $x_l = -a + b\eta$ whereas the upper one is $x_u = a + b\eta$. For a non-vanishing result, we need $x_l = -a + b\eta < x_F$. This will occur if $b_- < b < b_+$, where

$$b_\pm = \pm\frac{y_F}{2} + \sqrt{\frac{y_F^2}{4} + a(x_F + a)}. \tag{B 1}$$

Depending on whether $x_u < x_F$ or $x_u > x_F$, results for the imaginary part will differ. For $x_u = a + b\eta < x_F$, one needs $a < x_F$ and

$$b^2 - y_F b + a(x_F - a) < 0, \tag{B 2}$$
$$b^2 + y_F b + a(x_F - a) > 0. \tag{B 3}$$

To satisfy (B 2), the argument of the square-root appearing in the roots of the associated equation has to be positive, so that $0 < a < (x_F - 1)/2$ and $(x_F + 1)/2 < a < x_F$. Then, (B 3) will always be satisfied whereas (B 2) implies $\bar{b}_- < b < \bar{b}_+$, where

$$\bar{b}_\pm = \frac{y_F}{2} \pm \sqrt{\frac{y_F^2}{4} - a(x_F - a)}. \tag{B 4}$$

As a result, the integrals in (A 2) and (A 3), with the definition $[f(x)]_{x_l}^{x_u} \equiv f(x_u) - f(x_l)$, define regions (A) and (B) in § 3.3.

In case (iii) [$\chi^2 > 1$, $\eta < 1$ $(a > b > b\eta)$], the lower integration limit of (A 2), (A 3) is $x_l = a - b\eta$ whereas the upper one is $x_u = a + b\eta$. For a non-vanishing result, $x_l = a - b\eta < x_F$. This will always occur if $a < x_F$ whereas for $a > x_F$, $b'_- < b < b'_+$, where

$$b'_\pm = \pm\frac{y_F}{2} + \sqrt{\frac{y_F^2}{4} - a(x_F - a)}. \tag{B 5}$$

Again, depending on whether $x_u < x_F$ or $x_u > x_F$, results for the imaginary part will differ. For $x_u = a + b\eta < x_F$, $a < x_F$ and

$$b^2 - y_F b + a(x_F - a) > 0, \tag{B 6}$$
$$b^2 + y_F b + a(x_F - a) > 0. \tag{B 7}$$

To satisfy (B 6), the argument of the square-root appearing in the roots of the associated equation has to be positive, so that $0 < a < (x_F - 1)/2$ and $(x_F + 1)/2 < a < x_F$. Then, (B 7) will always be satisfied whereas (B 6) implies $\bar{b}'_- < b < \bar{b}'_+$, with

$$\bar{b}'_\pm = \frac{y_F}{2} \pm \sqrt{\frac{y_F^2}{4} - a(x_F - a)}. \tag{B 8}$$

We may then define regions (C) and (D) in § 3.3.

https://doi.org/10.1017/S0022377818000144 Published online by Cambridge University Press

Appendix C. Real parts at $T = 0$

The first integral in expressions (3.6) and (3.7) is simply

$$\tfrac{1}{2}[x_F y_F - \ln(x_F + y_F)], \tag{C 1}$$

whereas the last ones may be integrated by parts, using $R_1(1) = R_2(1) = 0$, to yield

$$\frac{x_F}{12b}[(x_F^2 + 3\chi^2)R_1(x_F) + 6ax_F R_2(x_F)] - \frac{1}{12b}\int_1^{x_F} \mathrm{d}x[(x^3 + 3\chi^2 x)R_1' + 6ax^2 R_2'], \tag{C 2}$$

for (3.6), and

$$\frac{x_F}{8b}(1 + 2\chi^2)R_1(x_F) - \frac{1}{8b}\int_1^{x_F} \mathrm{d}x(1 + 2\chi^2)xR_1', \tag{C 3}$$

for (3.7). It is convenient to introduce

$$L_\pm(x) \equiv \ln\left(\frac{|\pm ax + by + \chi^2|}{|\pm ax - by + \chi^2|}\right), \tag{C 4}$$

so that $R_1 = -(L_+ + L_-)$, $R_2 = -(L_+ + L_-)/2$. Taking derivatives, dividing out the resulting polynomials and adding the $\pm$ contributions leads to

$$\frac{x_F}{12b}[(x_F^2 + 3\chi^2)R_1(x_F) + 6ax_F R_2(x_F)] + \frac{1}{6}[x_F y_F + (3 - 4b^2)\ln(x_F + y_F)] + Z_B, \tag{C 5}$$

for (3.6) and

$$\frac{x_F}{8b}(1 + 2\chi^2)R_1(x_F) + \frac{1}{2}(1 + 2\chi^2)\ln(x_F + y_F) + Z_D, \tag{C 6}$$

for (3.7), with Z_B and Z_D defined and calculated in appendix D.

Appendix D. Definition and calculation of Z_B and Z_D

The explicit expressions of $Z_{B,D}$ are

$$Z_{B,D} = C_{B,D}\int_1^{x_F} \frac{\mathrm{d}x}{\sqrt{x^2 - 1}}\frac{M_{B,D}x^2 + N_{B,D}}{(x^2 + \zeta^2)^2 - 4a^2x^2}, \tag{D 1}$$

where $\zeta^2 \equiv a^2 - \eta^2 b^2$, $C_B = 1/3$ and $C_D = (1 + 2\chi^2)/2$. The expressions for $M_{B,D}$ and $N_{B,D}$ depend solely on a and b,

$$\left.\begin{aligned} M_B &= -2a^2(1 + 4b^2) - [1 - 2b^2 - 2a^2(2 - \eta^2)]\zeta^2, \\ N_B &= -\zeta^4(1 - 2b^2), \\ M_D &= 2a^2(1 + \eta^2) - \zeta^2, \\ N_D &= -\zeta^4. \end{aligned}\right\} \tag{D 2}$$

Defining $t = \sqrt{(x^2 - 1)/x^2} = y/x$, (D 1) reduces to

$$Z_{B,D} = C_{B,D}[(M_{B,D} + N_{B,D})\mathfrak{I}_0 - N_{B,D}\mathfrak{I}_2], \tag{D 3}$$

where $\mathfrak{I}_j$ is

$$\mathfrak{I}_j = \int_0^{t_F} \frac{\mathrm{d}t t^j}{\mathfrak{C}t^4 + \mathfrak{B}t^2 + \mathfrak{A}}, \tag{D 4}$$

https://doi.org/10.1017/S0022377818000144 Published online by Cambridge University Press

and the coefficients are $\mathfrak{C} = \zeta^4$, $\mathfrak{B} = -2[\zeta^2(\zeta^2+1) - 2a^2]$, and $\mathfrak{A} = (\zeta^2+1)^2 - 4a^2$. There are two cases to be considered, depending on the roots of the biquadratic equation $\mathfrak{C}t^4 + \mathfrak{B}t^2 + \mathfrak{A} = 0$:

(i) For $\eta^2 > 0$, the roots are real

$$t_\pm^2 = \frac{\zeta^2(\zeta^2+1) - 2a^2 \pm 2ab|\eta|}{\zeta^4}, \tag{D 5}$$

so that the integrals become

$$\mathfrak{I}_j = \frac{1}{4ab|\eta|}\left[t_+^j \int_0^{t_F} \frac{\mathrm{d}t}{t^2 - t_+^2} - t_-^j \int_0^{t_F} \frac{\mathrm{d}t}{t^2 - t_-^2}\right]. \tag{D 6}$$

One may show that $t_\pm^2 > 0$, therefore

$$\int_0^{t_F} \frac{\mathrm{d}t}{t^2 - t_\pm^2} = \frac{1}{2t_\pm} \ln\left|\frac{t_F - t_\pm}{t_F + t_\pm}\right|, \tag{D 7}$$

where, from (D 5), we may write $t_\pm = (y_\pm/|x_\pm|)$, with $x_\pm = a \pm b\eta$ and $y_\pm = \sqrt{x_\pm^2 - 1}$. Then,

$$\mathfrak{I}_0 = \frac{1}{4ab|\eta|}\left[\frac{1}{2t_+} \ln\left|\frac{t_F - t_+}{t_F + t_+}\right| - (t_+ \to t_-)\right], \tag{D 8}$$

$$\mathfrak{I}_2 = \frac{1}{4ab|\eta|}\left[\frac{t_+}{2} \ln\left|\frac{t_F - t_+}{t_F + t_+}\right| - (t_+ \to t_-)\right]. \tag{D 9}$$

(ii) For $\eta^2 < 0$, the roots are complex conjugate $(t_c^2, \bar{t}_c^2)$, with

$$t_c^2 = \frac{[\zeta^2(\zeta^2+1) - 2a^2] + \mathrm{i}[2ab|\eta|]}{\zeta^4}. \tag{D 10}$$

We may decompose into partial fractions to obtain $\mathfrak{I}_j = \mathfrak{I}_j^+ - \mathfrak{I}_j^-$ $(t_r \equiv \mathrm{Re}\, t_c;\ t_i \equiv \mathrm{Im}\, t_c)$

$$\mathfrak{I}_j^\pm = \frac{1}{4\zeta^4 t_r |t_c|^2} \int_0^{t_F} \left[\frac{\mathrm{d}t t^j (t \pm 2t_r)}{t^2 \pm 2t_r t + |t_c|^2}\right], \tag{D 11}$$

and write

$$\begin{aligned}\mathfrak{I}_0 \;=\; & \frac{1}{8\zeta^4 t_r |t_c|^2}\left\{\ln\left|\frac{t_F^2 + 2t_r t_F + |t_c|^2}{t_F^2 - 2t_r t_F + |t_c|^2}\right|\right. \\ & \left. + \frac{2t_r}{|t_i|}\left[\arctan\left(\frac{t_F + t_r}{|t_i|}\right) + \arctan\left(\frac{t_F - t_r}{|t_i|}\right)\right]\right\},\end{aligned} \tag{D 12}$$

as well as

$$\begin{aligned}\mathfrak{I}_2 \;=\; & \frac{1}{8\zeta^4 t_r}\left\{-\ln\left|\frac{t_F^2 + 2t_r t_F + |t_c|^2}{t_F^2 - 2t_r t_F + |t_c|^2}\right|\right. \\ & \left. + \frac{2t_r}{|t_i|}\left[\arctan\left(\frac{t_F + t_r}{|t_i|}\right) + \arctan\left(\frac{t_F - t_r}{|t_i|}\right)\right]\right\},\end{aligned} \tag{D 13}$$

where, from (D 10), one may show that $t_c = (y_c/x_c)$, with $x_c = a + \mathrm{i}b|\eta|$ and $y_c = \sqrt{x_c^2 - 1}$.

https://doi.org/10.1017/S0022377818000144 Published online by Cambridge University Press

REFERENCES

ABRIKOSOV, A. A., GORKOV, L. P. & DZYALOSHINSKI, I. E. 1975 *Methods of Quantum Field Theory in Statistical Physics*. Dover.

AHMED, K. & MASOOD, S. 1991 Vacuum polarization at finite temperature and density in qed. *Ann. Phys.* **207** (2), 460–473.

AKHIEZER, I. A. & PELETMINSKII, S. V. 1960 Use of the methods of quantum field theory for the investigation of the thermodynamical properties of a gas of electrons and photons. *Zh. Eksp. Teor. Fiz.* **11**, 1316–1322.

ASHCROFT, N. W. & MERMIN, N. D. 2005 *Solid State Physics*. Holt, Rinehart and Winston.

BARBARO, M. B., CENNI, R. & QUAGLIA, M. R. 2005 The generalised relativistic lindhard functions. *Eur. Phys. J.* A **25** (2), 299–318.

BARTON, G. 1990 On the finite-temperature quantum electrodynamics of free electrons and photons. *Ann. Phys.* **200** (2), 271–303.

BERRY, M. V. 2005 The optical singularities of bianisotropic crystals. *Proc. R. Soc. Lond.* A **461**, 2071–2098.

DE CARVALHO, C. A. A. 2016 Relativistic electron gas: a candidate for nature's left-handed materials. *Phys. Rev.* D **93** (10), 105005.

DONOGHUE, J. F., HOLSTEIN, B. R. & ROBINETT, R. W. 1985 Quantum electrodynamics at finite temperature. *Ann. Phys.* **164** (2), 233–276.

ELIASSON, B. & SHUKLA, P. K. 2011 Relativistic laser-plasma interactions in the quantum regime. *Phys. Rev.* E **83** (4), 046407.

FETTER, A. L. & WALECKA, J. D. 2012 *Quantum Theory of Many-particle Systems*. Courier Corporation.

GU, X.-Q., WANG, S.-Y. & YIN, W.-Y. 2014 Optical responses of planar composites consisting of monolayer graphene sheets and axially helicoidal (bi) anisotropic films. *Opt. Commun.* **313**, 9–14.

ITZYKSON, C. & ZUBER, J.-B. 2006 *Quantum Field Theory*. Courier Corporation.

JANCOVICI, B. 1962 On the relativistic degenerate electron gas. *Il Nuovo Cimento* **25** (2), 428–455.

KAPUSTA, J. I. & GALE, C. 2006 *Finite-temperature Field Theory: Principles and Applications*. Cambridge University Press.

LE BELLAC, M. 2000 *Thermal Field Theory*. Cambridge University Press.

LINDHARD, J. 1954 On the properties of a gas of charged particles. *Kgl. Danske Videnskab. Selskab Mat.-Fys. Medd.* **28**, 1–57.

MASOOD, S. & SALEEM, I. 2016 Propagation of electromagnetic waves in extremely dense media. *Intl J. Mod. Phys.* A 1750081.

MCORIST, J., MELROSE, D. B. & WEISE, J. I. 2007 Dispersion in a relativistic degenerate electron gas. *J. Plasma Phys.* **73** (4), 495–513.

MELROSE, D. B. & HAYES, L. M. 1984 Dispersion in a relativistic quantum electron gas. II. Thermal distributions. *Austral. J. Phys.* **37** (6), 639–650.

PENDRY, J. B. 2003 Focus issue: negative refraction and metamaterials. *Optics Express* **11** (7), 639–639.

PÉREZ ROJAS, H. & SHABAD, A. E. 1982 Absorption and dispersion of electromagnetic eigenwaves of electron-positron plasma in a strong magnetic field. *Ann. Phys.* **138** (1), 1–35.

PULSIFER, P. & KALMAN, G. 1992 Pair-creation collective modes in an electron gas. *Phys. Rev.* A **45** (8), 5820–5829.

REIS, D. M., REYES-GÓMEZ, E.-O. L. E. & DE CARVALHO, C. A. A. 2017 Electromagnetic propagation in a relativistic electron gas at finite temperatures. *Ann. Phys.* arXiv:1711.07818.

REYES-GÓMEZ, E., OLIVEIRA, L. E. & DE CARVALHO, C. A. A. 2016 The electromagnetic response of a relativistic fermi gas at finite temperatures: applications to condensed-matter systems. *Europhys. Lett.* **114** (1), 17009.

STURM, K. 1982 Electron energy loss in simple metals and semiconductors. *Adv. Phys.* **31** (1), 1–64.

STURM, K. & OLIVEIRA, L. E. 1980 High-frequency dielectric properties of covalent semiconductors within the nearly-free-electron approximation. I. The one-plasmon-band model. *Phys. Rev.* B **22** (12), 6268.

https://doi.org/10.1017/S0022377818000144 Published online by Cambridge University Press

STURM, K. & OLIVEIRA, L. E. 1981 Wave-vector-dependent plasmon linewidth in the alkali metals. *Phys. Rev.* B **24** (6), 3054.

TSAI, W.-Y. & ERBER, T. 1974 Photon pair creation in intense magnetic fields. *Phys. Rev.* D **10** (2), 492.

VESELAGO, V. G. 1968 The electrodynamics of substances with simultaneously negative values of and μ. *Sov. Phys. Uspekhi* **10** (4), 509.

WELDON, H. A. 1982 Covariant calculations at finite temperature: the relativistic plasma. *Phys. Rev.* D **26** (6), 1394.

https://doi.org/10.1017/S0022377818000144 Published online by Cambridge University Press